Multiport Network Model for CAD of Electromagnetically Coupled Microstrip Patch Antennas

Rajan P. Parrikar and Kuldip C. Gupta, *Fellow, IEEE*

***Abstract*— In this paper, electromagnetically coupled (EMC) patch-antenna configurations on two-layered dielectric substrates are investigated. The radiating patch is located on the top of the upper substrate and is excited by feed circuitry underneath it on the lower substrate. The electromagnetic field problem is transformed into a network problem and a multiport network model (MNM) is developed to characterize the three-dimensional (3-D) fields associated with the radiating structure. Antenna characteristics such as input impedance and radiation pattern are computed using the MNM model and the approach is validated by comparison with experimental results.**

***Index Terms*—Microstrip antennas, networks.**

I. Introduction

THE advent of sophisticated printed circuit techniques in recent years has spawned several novel circuit and antenna configurations, a major advance being the microstrip patch antenna [1]–[4]. In this work, a network model amenable to computer-aided analysis and design of a planar microstrip patch-antenna configuration employing two substrate layers, wherein the circuit elements are fabricated on the lower substrate and the radiating patches are located on the upper substrate, has been proposed. The excitation of the radiating patch is effected via electromagnetic coupling between the patch and the feed circuitry on the lower level underneath the patch. The advantages of using two-layer configurations are: 1) flexibility in design for optimizing both circuit and antenna parameters thus providing the best surface real estate usage; 2) an increase in radiated power and, consequently, increased bandwidth and efficiency [5], [6] caused by a larger patch-to-ground-plane spacing; and 3) a reduction in spurious radiation from the feed circuit discontinuities [7] resulting from the decrease in the spacing between the feed circuitry and the ground plane.

Two types of structures suitable for both hybrid and monolithic circuit integrations have been suggested recently [24]. A typical configuration suitable for hybrid integration is shown in Fig. 1. In this case, the thickness of the lower substrate (where the circuit elements are located) is much smaller than that of the upper layer. The lower substrate typically has a much higher dielectric constant than that of the upper layer.

Manuscript received November 27, 1995; revised November 26, 1997.

R. P. Parrikar is with the Antenna Engineering Department, Space Systems/Loral, Palo Alto, CA 94303 USA.

K. C. Gupta is with the University of Colorado, Boulder, CO 80309 USA.

Publisher Item Identifier S 0018-926X(98)02675-1.

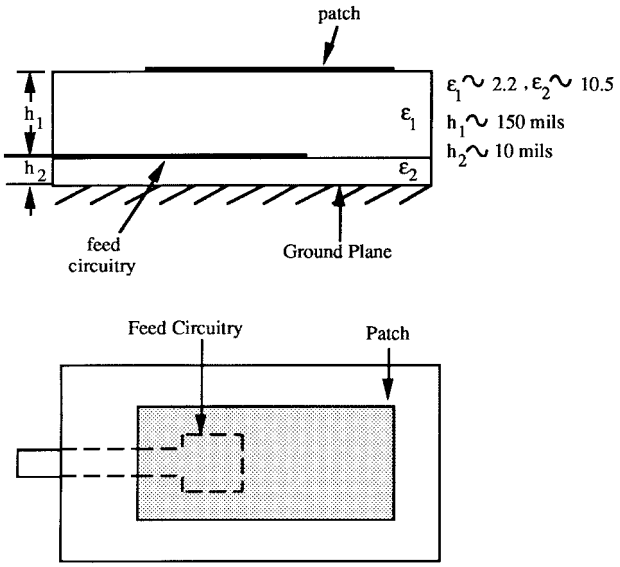

Fig. 1. A two-layer circuit-antenna configuration suitable for hybrid integration.

The feed circuitry is located on the lower substrate at the interface of the two layers. On the other hand, for antennas designed for integration with monolithic circuit configurations, the lower substrate is GaAs (about 100 to 150 μm thick) and the upper dielectric is a thin (1- to 2-μm) passivating layer (typically silicon nitride).

The early investigations into electromagnetically coupled (EMC) feed mechanisms for radiators considered printed microstrip dipoles [8], where various configurations of printed dipoles were examined for optimizing characteristics such as bandwidth, efficiency, and radiation. These studies employed both the circuit models using transmission line theory [1] as well as the rigorous moment method for EMC printed dipoles [9].

An experimental study of a proximity-coupled EMC microstrip patch antenna was presented in [10] with a demonstration of a bandwidth of 13%. The study also showed cross-polarization levels to be 20 dB below the copolarization levels. A generalized rigorous moment-method analysis to the problem of a rectangular microstrip patch antenna fed by a microstrip line was developed [11], [12] and measured and calculated results of the input impedance for the EMC antenna were reported. A similar type of moment-method analysis on

0018–926X/98$10.00 © 1998 IEEE

circular-patch antenna was carried out [13] and the effect of the line feed and patch overlap on the VSWR investigated. These full-wave analyses led to the development of guidelines for electromagnetically fed microstrip patch antennas for both the rectangular and circular shapes [14].

In the recent past, extensive experimental investigations into rectangular EMC patch antennas have been reported [15]–[17] along with detailed parametric studies.

The work reported herein takes a network approach known as the MNM technique. In Section II, some background and salient features of the MNM approach are enunciated. Section III deals with a detailed development of the MNM for the three-dimensional (3-D) fields associated with the EMC antenna configuration. In Section IV, the numerical results obtained by using MNM on sample cases and their validation by comparison with experimental results are presented. In Section V, a summary of this work is presented.

II. Analysis and Design Approach

There are several well-known techniques available for the analysis and design of microstrip patch antennas and they fall broadly in the following four groups, namely: 1) the transmission line model [1]; 2) the cavity model [18]; 3) electromagnetic full-wave techniques using numerical methods [19], [20]; and 4) the multiport network model technique [21]–[23].

In this paper, the MNM has been developed for the EMC patch antenna. The MNM was initially developed for analysis and design of single-layered microstrip patches at the University of Colorado at Boulder [21]–[23] and may be considered as an extension of the cavity model formalism [18]. Some of the key features of the MNM technique are: 1) it allows incorporation of feed junction reactances; 2) mutual coupling between the edges of the patch and other circuits nearby can be accounted for; 3) it is applicable to patches of composite shape; and 4) it allows application of network solution techniques making it ideal for CAD since it is computationally quicker and less expensive than full-wave analysis methods. The present paper extends the MNM approach to two-layered EMC patches.

III. The Multiport Network Model for the EMC Patch

For purposes of illustration of the development of MNM, the hybrid configuration ($h_2 \ll h_1$), shown in Fig. 2, is considered. In this two-layer EMC radiating patch configuration, the radiating patch is located on the top of the upper layer and excited by a microstrip line directly underneath the patch on the interface of the two substrates.

The MNM has been used extensively for the analysis and design of single-layer microstrip patch antennas and arrays [22]. This approach essentially converts the electromagnetic boundary value problem of the radiating configuration into an equivalent network problem and the entire structure is characterized by three (or more) interconnected multiport subnetworks.

The MNM has been used hitherto for the analysis and design of single-layer microstrip patches fed by microstrip lines in direct contact with the patch of by coaxial feeds [22]. In either of these two cases, the fields underneath the radiating patch are essentially invariant along the z direction (that is, in the direction perpendicular to the ground plane). In the present EMC antenna configuration, the fields underneath the radiating patch, however, vary in all the three mutually orthogonal directions. Hence, the MNM developed in this paper has to account for these field variations. Furthermore, the electromagnetic coupling mechanism from the feedline to the radiating patch calls for a different viewpoint and approach to modeling of the excitation. These factors invite development of a MNM that is a significant extension of the earlier version of the MNM developed for single-layer patches so as to accurately characterize the EMC antenna structure encountered here.

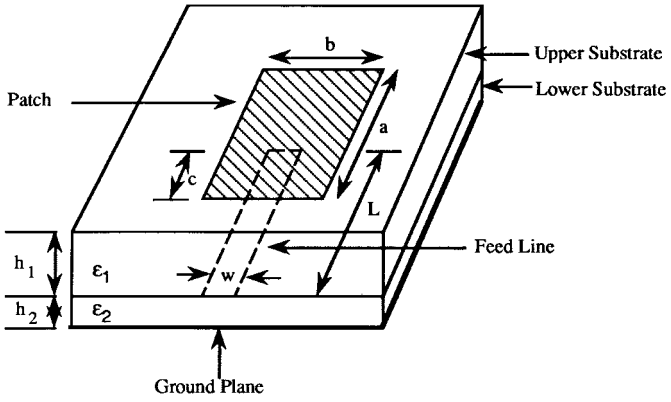

Fig. 2. The two-layer EMC patch configuration.

The fields associated with the feed structure and the radiating patch are identified and modeled separately by their respective subnetwork components. The fields responsible for the radiated power and the power loss due to surface waves are also delineated and modeled by another subnetwork component, which is characterized by an equivalent Z matrix. Finally, the subnetworks are combined to construct the overall network model of the radiating configuration and the relevant antenna characteristics such as the input impedance and radiation pattern are then determined from the overall network model. Each of the subnetworks will now be discussed separately.

A. The Patch Network

The modal field distribution in the region underneath the patch resembles that of a resonant electromagnetic cavity. The patch network (PN) models the electromagnetic fields in this region by viewing it as a two-layer open cavity that is surrounded by perfect magnetic walls (zero-tangential magnetic field) on the sides and perfect electric walls (zero-tangential electric field) on the top and bottom, as shown in Fig. 3. The electromagnetic field distribution in the cavity is expanded in terms of an infinite series of 3-D field modes satisfying the boundary conditions at the cavity walls. The fields associated with the metallic feed structure are considered as equivalent "sources" for the fields associated with the radiating patch. With this viewpoint, it follows that the coupling from the

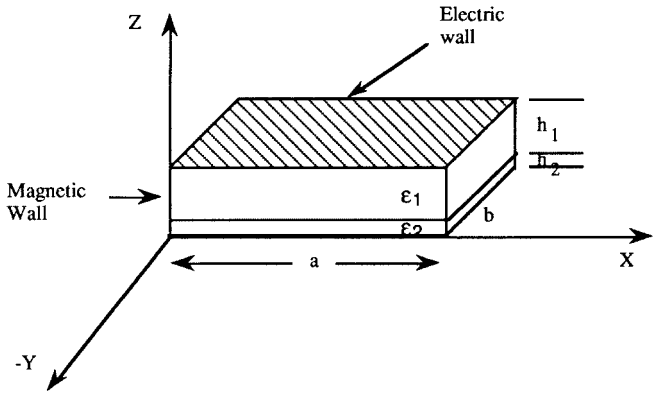

Fig. 3. A two-layer open electromagnetic cavity.

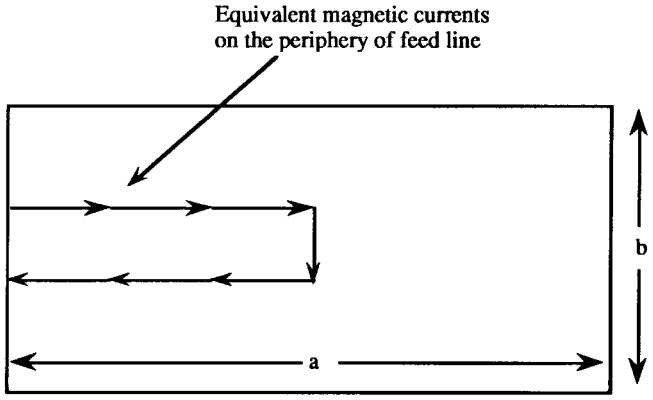

Fig. 4. Equivalent magnetic currents on feedline periphery.

feed structure to the radiating patch is via equivalent sources representing the fields of the feed structure [24].

The equivalent sources for excitation of the patch are obtained by placing equivalent magnetic current elements at the periphery of the feed structure, as shown in Fig. 4, by application of the Schelkunoff equivalence theorem [25], [26]. In applying the equivalence principle to a region of interest, that region is further divided into two parts: the "source region," where the actual sources are known to reside, and the external "field region," where the field produced by the actual sources is to be evaluated. The "source region" is then bounded by a closed surface, also known as the "Schelkunoff surface," and equivalent electric currents ($\mathbf{J} = \mathbf{n} \times \mathbf{H}$) and magnetic currents ($\mathbf{M} = \mathbf{E} \times \mathbf{n}$) are placed on it. The closed Schelkunoff surface has to be chosen judiciously so that the application of the equivalence theorem can facilitate the computation of the fields due to the actual sources.

In Fig. 5, the feedline penetrating the two-layer cavity is denoted by BCGF and, hence, the source region can be identified to be that enclosed by the rectangular box denoted by ABCDEFGH and the field region is the volume enclosed by the rest of the open cavity. The Schelkunoff surface, therefore, is chosen to be that which encloses the rectangular box ABCDEFGH (excluding the face denoted by ABFE). Using Love's equivalence principle [26] (a form of the Schelkunoff equivalence theorem), the volume enclosed by the Schelkunoff surface is replaced by a perfect electric conductor. The perfect

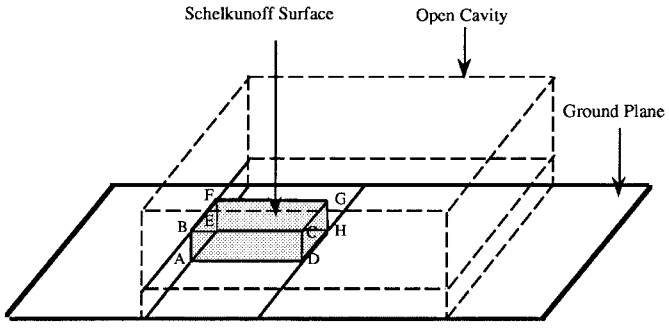

Fig. 5. Application of Schelkunoff equivalence theorem.

electric conductor placed therein nullifies the effect of the equivalent electric current elements on the Schelkunoff surface with the implication that only equivalent magnetic current elements need be placed on the Schelkunoff surface. The portion of the Schelkunoff surface denoted by BCGF coincides with the metallic feedline with the result that the tangential electric field on it vanishes. Hence, the equivalent magnetic current elements on that portion of the surface are zero. The primary sources of excitation to the open cavity are then the electric fields along the periphery of the feedline tangential to the surfaces ABCD, EFGH, and CDHG. To account for these tangential electric fields, equivalent magnetic current elements given by $\mathbf{M} = \mathbf{E} \times \mathbf{n}$ are placed along the periphery of the feedline, as shown earlier in Fig. 4. Since the feedline in this configuration lies very close to the ground plane ($h_2 \ll h_1$), the magnetic current distribution may be visualized as being localized in the ground plane along the periphery of the feed structure. The foregoing discussion for application of the Schelkunoff equivalence theorem applies to the hybrid configuration such as the one shown in Fig. 1. To use it on a monolithic configuration (where $h_1 \ll h_2$), a different Schelkunoff surface must be selected [24].

The development of the Z matrix for the PN follows from the analysis of the cavity fields. In the first step, the edges of the patch are subdivided along its physical periphery into smaller segments and ports are placed on each of these segments. The number of segments is determined by examination of the field variation along the edges of the patch. If the field varies rapidly along a patch edge, a large number of ports must be placed along it so that the variations are accurately accounted for. Typically, however, the patch is excited at a frequency that is in the vicinity of its dominant mode (TM_{100}) resonance for which the field distribution along the radiating edges is uniform. Therefore, the number of ports along the radiating edges in this case is kept to a minimum to reduce the computation time, the actual number determined iteratively so that numerical convergence is ensured. The edges of the feed structure are also subdivided into a number of smaller segments and ports are located on each of them. The locations of the ports in this case represent the presence of equivalent magnetic current sources.

A schematic diagram showing the placement of ports along the patch and the feedline is shown in Fig. 6. The fields at the "patch ports" due to a magnetic current element at a "feed port" are computed and a hybrid matrix representation

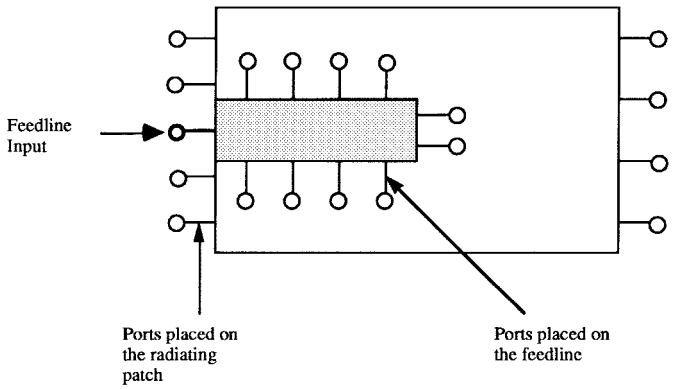

Fig. 6. Ports placement on the patch and feedline.

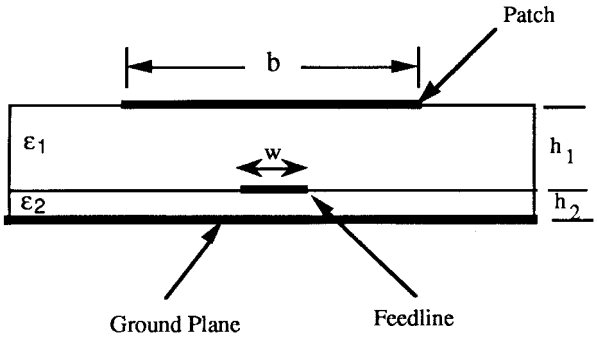

Fig. 7. Cross-sectional view of patch and feedline.

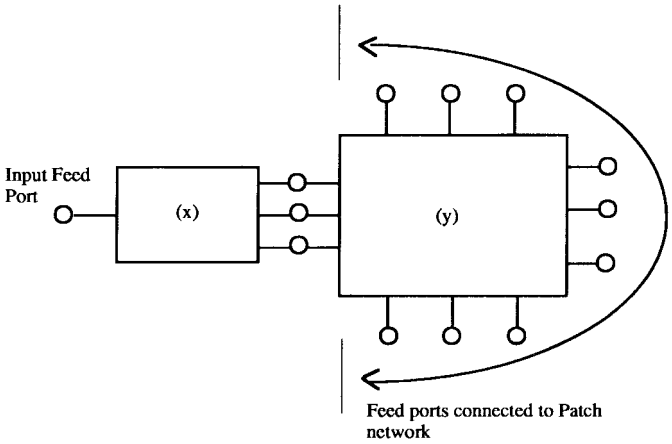

Fig. 8. Block diagram of the feed network.

of this relationship is obtained. The Z matrix is obtained by an appropriate transformation of the hybrid matrix [24].

It was stated that the region underneath the radiating patch is treated as a two-layer open cavity. The exact field solution for the resonance frequencies of modes of a two-layer cavity entails calculating the roots of a transcendental equation in the complex plane [27] and the resulting numerical work is cumbersome and computationally intensive. To get around this problem, an effective dielectric constant, which allows the two-layer cavity to be treated as a homogeneously filled single layer structure, may be defined by a simple expression of the form (refer to Fig. 3) [24] $\varepsilon_{\text{eff}} = \varepsilon_1\varepsilon_2(h_1 + h_2)/(\varepsilon_1 h_1 + \varepsilon_2 h_2)$.

B. The Feed Network

The The feed network (FN) characterizes the fields associated with the feed structure located at the interface of the two layers.

Refer once again to the configuration of Fig. 2, where the patch is excited by a simple feedline underneath it. A cross section of this arrangement, shown in Fig. 7, shows a resemblance to a two-layer asymmetric stripline configuration with the feedline, bound on the top and the bottom by the patch and the ground plane, respectively. This suggests that the feedline configuration may be treated as a transmission line structure supporting the quasi-TEM mode of propagation. The asymmetric stripline configuration is analyzed by using the static spectral domain technique [28]–[30] and its parameters such as the effective dielectric constant and the characteristic impedance are obtained. An equivalent planar waveguide model is then constructed from these parameters [31] and two-dimensional (2-D) planar analysis is used to compute the Z matrix of the feed structure.

A typical FN will have one port at the input and several output ports which get connected to the input ports of the PN. The FN itself may consist of two or more subnetworks depending upon the layout of the feed configuration as shown in Fig. 8. In this figure, segment "y" represents the planar waveguide model for the portion of the feed structure underneath the patch and the ports of this segment are connected to the ports of the PN. Segment "x" represents the short section of microstrip line outside the patch, as is usually the case for a practical configuration.

This modeling approach is valid for other variations of the feed network also. An interesting example is of a resonant feeder patch located on the lower substrate to act as a source of excitation of the radiating patch on the upper substrate. This feeder patch is designed to have dimensions that are smaller than and a resonance frequency close to that of the radiating patch. These objectives can be met if the lower substrate has a higher dielectric constant than the upper one.

C. The Edge-Admittance Network

The edge-admittance network (EAN) models the fields external to the patch, namely, the fringing fields, the radiated field, and the surface-wave field. The EAN is connected to the edge ports of the PN.

The EAN for each edge of the radiating patch is identical to that for single-layer patches [21]. It consists of combinations of capacitances (to account for the fringing electric field), inductances (to account for the fringing magnetic field) and conductances (to account for the radiated power and surface-wave loss). A section of the EAN is shown in Fig. 9.

The edge conductance of the EAN accounts for the power flow by two different mechanisms, viz., radiation and surface-wave loss. It has been shown [2] that the surface-wave power loss is relatively small and may be neglected for electrically thin substrates and, hence, the major contribution to the edge conductance is considered to come from the radiated power. The edge conductance is an equivalent ohmic conductance whose value is such that it dissipates a power equal to that

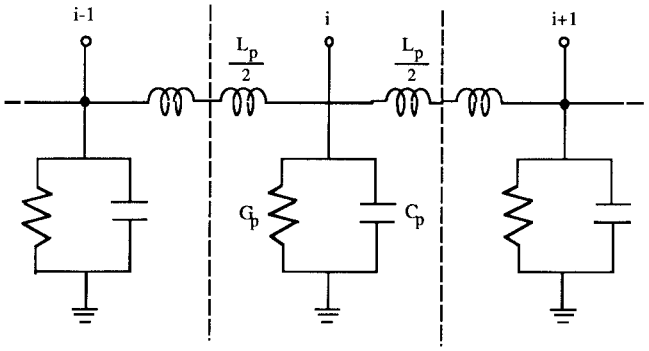

Fig. 9. Section of the edge-admittance network.

radiated by the edge of the patch. If the voltage distribution along an edge is given by $f(x)$, the edge conductance G_r is given by [21]

$$G_r = \frac{2P_r}{\frac{1}{W}\int_0^W f^2(x)\,dx} \tag{1}$$

where x is the distance along the edge of the patch and P_r is the radiated power calculated for a voltage distribution $f(x)$.

Typically, the edge of the patch is divided into "n" uniformly spaced segments with ports placed on each one of them. The edge conductance connected to each of these ports is distributed uniformly and, hence, is equal to G_r/n. This method for calculation of the edge conductance requires an *a priori* knowledge of the voltage distribution along the edge of the patch. If the patch is operated in the vicinity of its dominant resonance frequency, the voltage distribution along the two radiating edges is constant and the above integral may be easily evaluated. However, for frequencies away from resonance, the calculation of the integral leads to inaccuracies due to the change in voltage distribution along the edge of the patch. To overcome this limitation in the edge-conductance model, another formulation has been developed recently and is known as the generalized edge-conductance network [32].

In the new edge-conductance model, the radiating edge is divided into a number (N_e) of small sections, each of width W_e. It may be noted that because of the mutual coupling among various sections, the total radiated power is not equal to the sum of the power radiated from each individual sections. The self-conductance terms g_{ii} are given by [2]

$$g_{ii} = \frac{W_e^2}{90\lambda_0^2} \tag{2}$$

where λ_0 is the free-space wavelength.

The edge conductance terms due to mutual coupling between various sections of the edge are evaluated by examining the interaction between two infinitesimally small magnetic current elements [24].

The edge capacitance of the EAN accounts for the energy stored in the fringing electric field at the edges of the patch. The fringing capacitance is defined as the excess of the total capacitance of the patch over that which would exist if the patch is considered as a 2-D capacitor with magnetic walls at the open edges. The edge capacitance is distributed uniformly

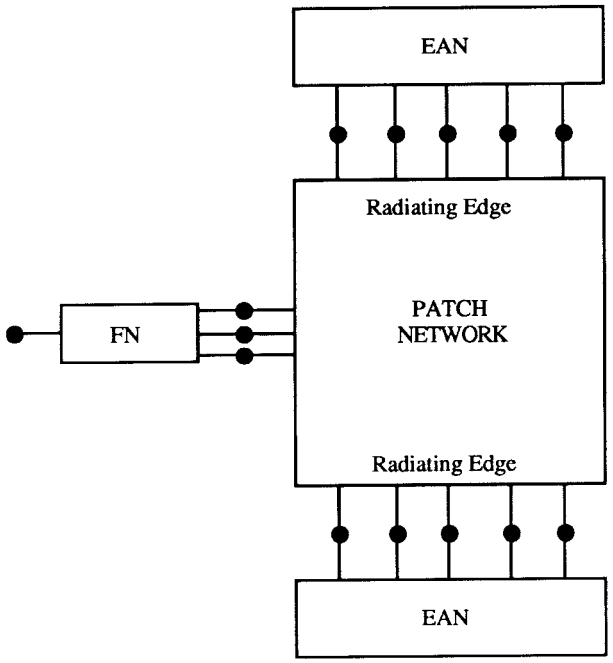

Fig. 10. Overall multiport network model of the configuration.

over the n ports of the edge in the same manner as the edge conductance in the former of the two edge-conductance models discussed earlier.

Closed-form expressions are available for computation of the edge capacitance. These expressions are usually derived from rigorous hybrid mode-matching solutions which are then curve fitted [33].

The edge inductance accounts for the energy stored in the fringing magnetic fields at the edge of the patch. When the patch antenna is operated near the dominant resonance frequency, as is usually the case, the voltage distribution along the edge is uniform and, hence, the voltages at the adjacent ports are equal. Therefore, there is no current flow through the edge inductance of Fig. 9 and it need not be included in the EAN network.

D. The Overall Network

Once the subnetworks have been characterized the overall network model of the radiating configuration is obtained by connecting the three networks (PN, FN, and EAN) together. The three Z matrices representing the PN, FN, and EAN are combined using the segmentation method [34], [35]. The procedure results in a Z matrix (1×1), which represents the input impedance of the antenna structure. The overall network model is shown in Fig. 10.

The segmentation method also gives the voltages at the PN–EAN connected ports. The voltage distribution so obtained is expressed as an equivalent magnetic current distribution and is used for the computation of the radiation field and the far-field patterns of the radiating configuration.

E. Hybrid Matrix for PN

The objective of the field analysis for the region underneath the radiating patch is to obtain the Z-matrix characterization

of the PN which models the interaction among the "patch ports" and the "feed ports." This process is simplified by the introduction of an intermediate calculation wherein a hybrid matrix is first computed.

This hybrid matrix relating voltages and currents at the feed and the patch ports is defined by [24]

$$\begin{bmatrix} \hat{V}_E \\ \hat{I}_F \end{bmatrix} = \begin{bmatrix} [H_{1\,1}][H_{1\,2}] \\ [H_{2\,1}][H_{2\,2}] \end{bmatrix} \begin{bmatrix} \hat{V}_F \\ \hat{I}_E \end{bmatrix} \tag{4}$$

where

$\hat{V}_E$ vector containing the edge port voltages;
$\hat{I}_E$ vector containing the edge port currents;
$\hat{V}_F$ vector containing the feed port voltages;
$\hat{I}_F$ vector containing the feed port currents.

The submatrix $[H_{11}]$ relates the voltages at the edge ports to the impressed voltages at the feed ports. $[H_{12}]$ links the edge-port voltages to the edge-port currents with the feed port shorted. In this state the fields underneath the patch may be considered to have no variation in the z direction and the configuration can, therefore, be treated as a 2-D planar structure and its Z matrix can be computed from Green's function analysis [31], [34]. $[H_{21}]$ relates the currents and voltages at the feed ports with the edge ports open and 3-D analysis is used to obtain this submatrix. $[H_{22}]$ relates the currents at the feed ports due to the impressed currents at the edge ports with the feed ports shorted and 2-D analysis is applicable to its computation.

The Z matrix for the PN is obtained from the hybrid matrix by simple matrix manipulation [24].

IV. Numerical Results and Discussion

A. Segmentation and Far-Field Calculations

Once the Z matrices of the FN, the PN, and the EAN are evaluated, they are combined by using the segmentation method [24], [34], [35] to yield the overall [1 × 1] impedance matrix of the radiating structure (Fig. 10). The segmentation procedure also yields the voltages at the edge ports so that the far-field radiation patterns of this configuration can be calculated.

In this section, the results obtained by using the MNM model for EMC patch antennas fed by a simple feedline are compared with those obtained by full-wave analysis and experimental results from literature. The generic configuration of Fig. 2 is investigated.

B. Comparison of MNM Results with PMesh Full-Wave Analysis

The configuration of Fig. 2 was analyzed by using both the MNM approach discussed in this paper and PMesh, a full-wave moment method analysis algorithm [20] developed at the University of Colorado at Boulder. The comparison for the input reflection coefficient S_{11} is shown in Fig. 11 for the following physical and electrical parameters: $a = 2.5$ cm, $b = 4$ cm, $c = 1.25$ cm, $w = 5$ mm, $\varepsilon_1 = \varepsilon_2 = 2.2$, and $h_1 = h_2 = 1.58$ mm.

The resonance frequency using the Pmesh code was found to be 3.62 GHz with a bandwidth of 4.6%, while the MNM technique gave a resonance frequency of 3.63 GHz with a corresponding bandwidth of 3.9%. (The bandwidth is defined for the range wherein VSWR $\leq$ 2.) The calculation of the reflection coefficient was in the plane perpendicular to the patch edge and the feedline of Fig. 2. The results show that the MNM approach gives a fairly accurate prediction of the resonance behavior of the antenna.

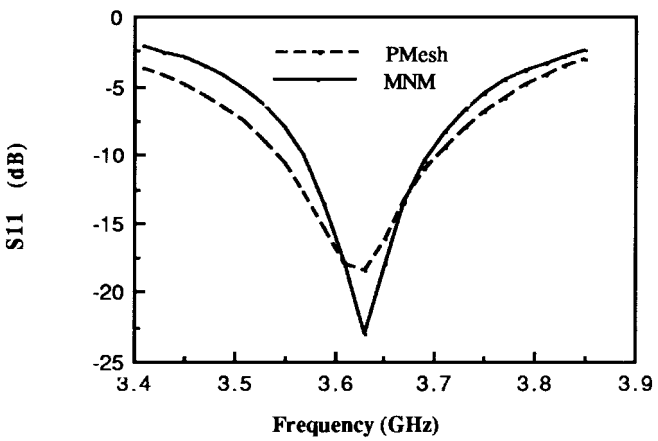

Fig. 11. $S_{1\,1}$ versus frequency—Pmesh and MNM.

C. Parametric Studies and Comparison with Experimental Results

In this section, the effects of the change in width of the radiating patch, the dielectric constants of the substrates and the width of the feedline on the input impedance and the reflection coefficient, are presented.

1) Effect of Patch Width on Input Impedance: The dependence of the input impedance of the EMC patch antenna configuration on the patch-feedline overlap (c/a), with the patch width as a variable parameter, is investigated in this subsection. The physical and electrical characteristics of the structure studied are (see Fig. 2): $a = 2.22$ cm, $w = 2.4$ mm, $L = 7.61$ cm, $h_1 = 1.5874$ mm, $h_2 = 0.794$ mm, $\varepsilon_1 = 2.2$, and $\varepsilon_2 = 2.33$.

This case has been subjected to extensive experimental investigation [17] and will be used to validate the MNM model that has been developed in this paper.

Fig. 12(a) shows the variation in the real part of the input impedance for a patch width $b = 1$ cm. The experimental value of the input impedance is seen to peak at around $c = 45\%$ whereas the value obtained by MNM reaches a maximum at $c = 50\%$. Similar curves are shown for patch widths of $b = 2$ cms and $b = 3$ cms in Fig. 12(b) and (c), respectively. The three plots are now presented in a composite form in Fig. 13. The curves for these physical dimensions indicate that a 50-Ω match is attainable for patch widths lying in the 1–2 cm range. Accordingly, the patch width may be varied along with the patch-feedline overlap to get the desired input impedance match.

2) Effect of Patch Width on Resonance Frequency: The effect of changes in the patch width on the resonance frequency of the patch antenna is presented in Table I. The results of MNM analysis are juxtaposed with the experimental results.

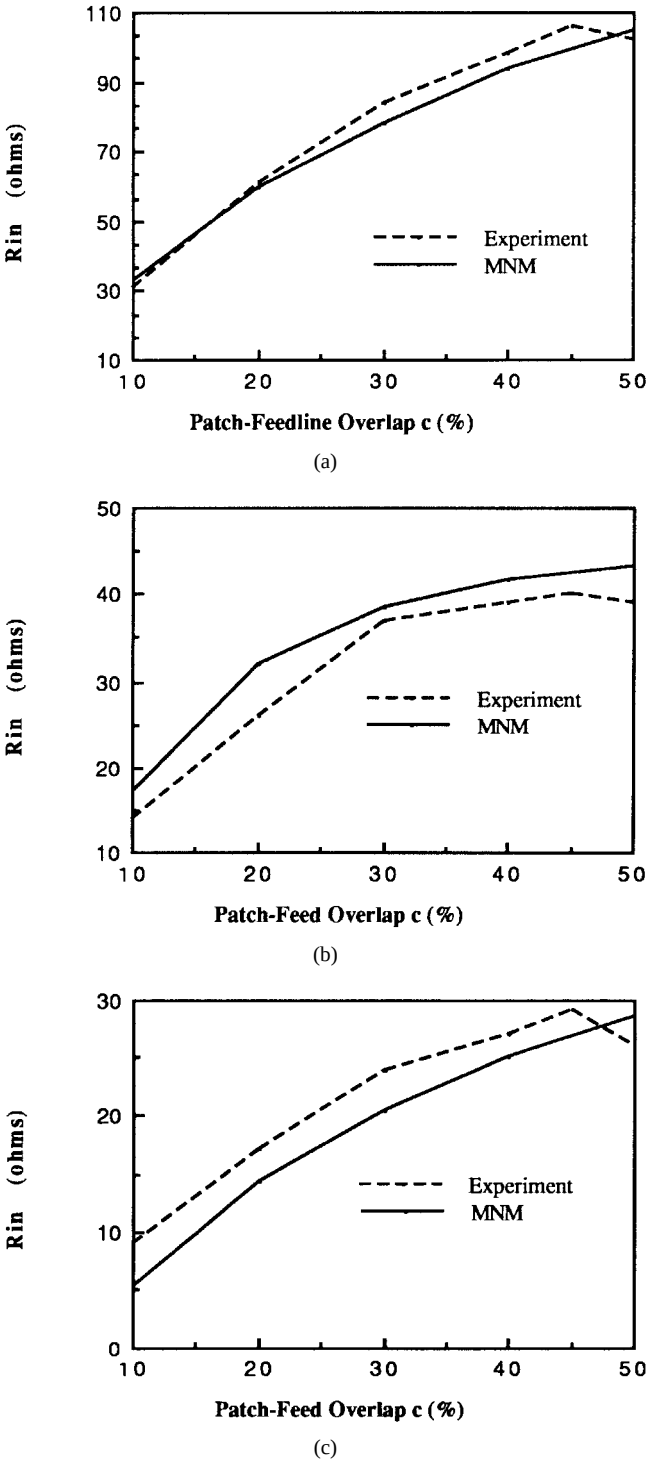

Fig. 12. (a) Real part of input impedance with patch-feedline overlap for $b = 1$ cm. (b) Real part of input impedance with patch-feedline overlap for $b = 2$ cm. (c) Real part of input impedance with patch-feedline overlap for $b = 3$ cm.

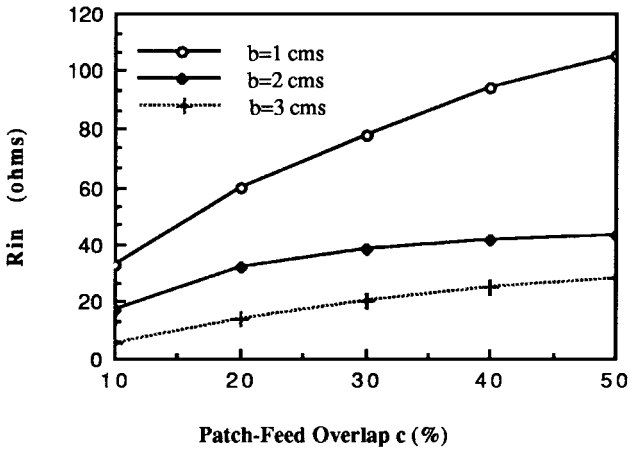

Fig. 13. Real part of input impedance with patch-feedline overlap for $b = 1$, 2 and 3 cm using MNM.

TABLE I
COMPARISON OF RESONANCE FREQUENCY MNM WITH EXPERIMENT ($c = 50\%$)

b (cm)	f_{exp} (GHz)	f_{MNM} (GHz)	% difference
1	4.28	4.31	0.7
2	4.10	4.16	1.46
3	4.02	4.10	1.99

TABLE II
EFFECT OF FEEDLINE WIDTH ON RESONANCE FREQUENCY AND INPUT IMPEDANCE USING THE MNM ($b = 1$ cm, $c = 50\%$)

w (cm)	f_r (GHz)	R_{in} (ohms)
0.15	4.315	76.5
0.20	4.310	94.6
0.24	4.310	105.0
0.30	4.310	107.3

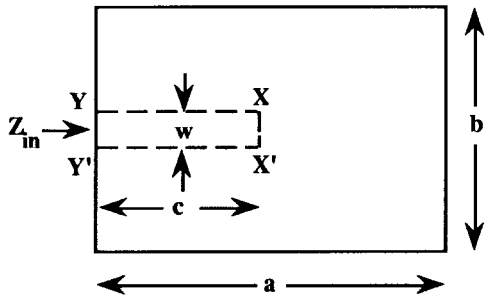

Fig. 14. Patch-feedline topology.

It is observed that as the patch width increases the resonance frequency decreases monotonically.

3) Effect of Feedline Width: The width of the feedline is an important parameter in the EMC patch antenna since it affects both the characteristic impedance of the input line as well as the excitation voltage. The dependence of the input impedance of the antenna with feedline width "w" is presented in Table II for a patch width of $b = 1$ cm and a patch-feedline overlap of $c = 50\%$. $R_{\rm in}$ represents the real part of the input impedance (at the input of the feedline of length "c") at the resonance frequency. As a first step in the process of obtaining a value of 50 Ω for $R_{\rm in}$, $Z_{\rm in}$ at the plane XX$'$ (see Fig. 14) with a given width of feedline is calculated and the value is then impedance transformed to the location of the input. It is seen that the resonance frequency is relatively unaffected by the width of the feedline, while the input impedance in the case cited increases with an increase in "w."

4) Effect of Substrate Dielectric Constants on S_{11}: The final part of this parametric study is an examination of the

TABLE III
EFFECT OF SUBSTRATE DIELECTRIC CONSTANT USING MNM FOR PATCH-FEEDLINE OVERLAP $c = 50\%$

	$\varepsilon_2 = 2.2$		$\varepsilon_2 = 2.33$	
b (cm)	$S_{11\min}$ (db)	f_r (GHz)	$S_{11\min}$ (db)	f_r (GHz)
1	-11.4	4.33	-15.05	4.31
2	-14.16	4.21	-20.4	4.16
3	-8.01	4.15	-12.76	4.10

effect of the dielectric constant (ε_2) of the lower substrate on antenna performance. The data in Table III indicates that a higher value of ε_2 (for the lower layer) yields a better match. The resonance frequency is also seen to decrease as expected with an increase in ε_2. For the same width, an increase in ε_2 decreases Z_0 of the feedline. Also, $\varepsilon_{\rm re}$ of the patch cavity is increased and hence the patch f_r is lowered. Table III shows that the patch was not well matched with the original feedline.

D. Radiation Pattern Calculations

The far-field radiation patterns for the rectangular EMC patch antennas are similar to those of the single layer microstrip line-fed antennas since it is essentially the shape of the radiating patch along with its mode of operation that determines the far-field pattern.

V. CONCLUSIONS

In this paper, an MNM has been developed for the analysis and design of EMC rectangular patch antenna configurations. The MNM essentially involves a transformation of the electromagnetic field problem into an equivalent circuit problem which can then be handled by the powerful techniques of network analysis to calculate the desired parameters. The primary advantage of this approach is its relatively simpler formulation over full-wave analysis and the resulting computational economy.

The MNM model developed for an EMC patch antenna has been validated by comparing it against a full-wave analysis algorithm as well as experimental data. The patch shape that is used to develop the model is rectangular but the approach is general and shape independent. The MNM model can be used with minor modifications to analyze number of other types of configurations such as patches excited by slots or by coplanar waveguides, or patches fed by resonant feeder patches located underneath them.

ACKNOWLEDGMENT

The authors would like to thank the reviewers for their keen comments and suggestions toward improving the clarity of this paper.

REFERENCES

[1] I. Bahl and P. Bhartia, *Microstrip Antennas.* Dedham, MA: Artech House, 1980.
[2] J. James, P. S. Hall, and C. Wood, *Microstrip Antenna Theory and Design.* London, U.K.: Peter Peregrinus, 1981.
[3] K. C. Gupta and A. Benalla, *Microstrip Antenna Design.* Norwood, MA: Artech House, 1988 (reprint volume).
[4] K. R. Carver and J. W. Mink, "Microstrip antenna technology," *IEEE Trans. Antennas Propagat.*, vol. AP-29, pp. 2–24, Jan. 1981.
[5] L. Lewin, "Radiation from discontinuities in stripline," *Proc. Inst. Elect. Eng.*, vol. 107C, pp. 163–170, Feb. 1960.
[6] C. Wood, P. S. Hall, and J. James, "Radiation conductance of open-circuit low dielectric constant microstrip," *Electron. Lett.*, vol. 14, pp. 121–123, Feb. 1978.
[7] M. D. Abouzahra and L. Lewin, "Radiation from microstrip discontinuities," *IEEE Trans. Microwave Theory Tech.*, vol. 27, pp. 722–723, Aug. 1979.
[8] H. G. Oltman and D. A. Huebner, "Electromagnetically coupled microstrip dipoles," *IEEE Trans. Antennas Propagat.*, vol. AP-29, pp. 151–157, Jan. 1981.
[9] P. B. Katehi and N. G. Alexopoulos, "On the modeling of electromagnetically coupled microstrip antennas—The printed strip dipole," *IEEE Trans. Antennas Propagat.*, vol. AP-32, pp. 1179–1186, Nov. 1984.
[10] D. M. Pozar and B. Kaufman, "Increasing the bandwidth of a microstrip antenna by proximity coupling," *Electron. Lett.*, vol. 23, pp. 368–369, Apr. 1987.
[11] D. M. Pozar and S. M. Voda, "A rigorous analysis of a microstrip fed patch antenna," *IEEE Trans. Antennas Propagat.*, vol. AP-35, pp. 1343–1350, Dec. 1987.
[12] H. Legay, J. Floc'h, J. Citerne, and G. Piton, "Etude theorique et experimentale d'antennas plaques alimentees par couplage de proximite a une line microruban," *Ann. Telecommun.*, vol. 45, no. 3–4, pp. 192–202, 1990.
[13] M. Davidovitz and Y. T. Lo, "Rigorous analysis of a circular patch antenna excited by a microstrip transmission line," *IEEE Trans. Antennas Propagat.*, vol. 37, pp. 949–958, Aug. 1989.
[14] G. Splitt and M. Davidovitz, "Guidelines for design of electromagnetically coupled patch antennas on two-layer substrates," *IEEE Trans. Antennas Propagat.*, vol. 38, pp. 1136–1140, July 1990.
[15] J. S. Roy, S. K. Shaw, P. Paul, D. R. Poddar, and S. K. Chowdhury, "Some experimental investigations on electromagnetically coupled microstrip antennas on two-layer substrates," *Microwave Opt. Tech. Lett.*, vol. 4, pp. 236–238, May 1991.
[16] N. C. Karmakar and A. Bhattacharya, "Electromagnetically coupled patch antenna—Theoretical and experimental investigations," *Microwave Opt. Tech. Lett.*, vol. 5, pp. 115–118, Mar. 1992.
[17] N. C. Karmakar and M. E. Bialkowski, "Experimental investigations into an electromagnetically coupled microstrip patch antenna," *Microwave Opt. Tech. Lett.*, vol. 5, pp. 447–453, Aug. 1992.
[18] Y. T. Lo, D. Solomon, and W. F. Richards, "Theory and experiment on microstrip antennas," *IEEE Trans. Antennas Propagat.*, vol. AP-27, pp. 137–145, Mar. 1979.
[19] R. C. Booton, Jr., *Computational Methods for Electromagnetics and Microwaves.* New York: Wiley, 1992.
[20] D. C. Chang and J. X. Zheng, "Electromagnetic modeling of passive circuit elements in MMIC," *IEEE Trans. Microwave Theory Tech.*, vol. 40, pp. 1741–1747, Sept. 1992.
[21] K. C. Gupta, "Multiport network approach for modeling and analysis of microstrip patch antennas and arrays," in *Handbook of Microstrip Antennas*, J. R. James and P. S. Hall, Eds. London, U.K.: Peter Peregrinus, 1989, vol. 1, pp. 455–526.
[22] ———, "Multiport network modeling approach for computer-aided design of microstrip patches and arrays," in *IEEE Antennas Propagat. Int. Symp.*, Blacksburg, VA, June 1987, pp. 786–789.
[23] A. Benalla and K. C. Gupta, "Multiport-network model and transmission characteristics of two-port rectangular microstrip antennas," *IEEE Trans. Antennas Propagat.*, vol. 36, pp. 1337–1342, Oct. 1988.
[24] R. P. Parrikar, "Network modeling of electromagnetically coupled and active microstrip patch antennas," Ph.D. dissertation, Dept. Elect. Comput. Eng., Univ. Colorado, Boulder, 1993.
[25] R. Harrington, *Time Harmonic Electromagnetic Fields.* New York: McGraw-Hill, 1961.
[26] C. Balanis, *Advanced Engineering Electromagnetics.* New York: Wiley, 1989.
[27] R. Collins, *Field Theory of Guided Waves.* New York: IEEE Press, 1991.
[28] H. Lee and V. K. Tripathi, "Generalized spectral domain analysis of planar structures having semi-infinite ground planes," in *IEEE Microwave Theory Tech. Int. Symp. Dig.*, San Francisco, CA, May 30–June 1, 1984, pp. 327–329.
[29] R. T. Kollipara and V. K. Tripathi, "Quasi-TEM spectral domain technique for multiconductor structures with rectangular and trapezoidal

conductor cross-section," *Microwave Opt. Tech. Lett.,* vol. 3, pp. 4–6, Jan. 1990.
[30] R. Crampagne, M. Ahmadpanah, and J. Guiraud, "A simple method for determining the Green's function for a large class of MIC lines having multilayered dielectric substrates," *IEEE Trans. Microwave Theory Tech.,* vol. MTT-26, pp. 82–87, Feb. 1978.
[31] T. Okoshi, *Planar Circuits for Microwaves and Lightwaves.* New York: Springer-Verlag, 1985.
[32] A. Benalla and K. C. Gupta, "A generalized edge admittance network for modeling of radiation from microstrip patch antennas," in *URSI Radio Sci. Meet.,* Boulder, CO, Jan. 1992, p. 65.
[33] M. Kirschning, R. H. Jansen, and N. H. L. Koster, "Accurate model for open end effect of microstrip lines," *Electron. Lett.,* vol. 17, pp. 123–125, Feb. 1981.
[34] K. C. Gupta, R. Garg, and R. Chadha, *Computer-Aided Design of Microwave Circuits.* Dedham, MA: Artech House, 1981.
[35] K. C. Gupta and P. C. Sharma, "Segmentation and desegmentation techniques for analysis of two-dimensional microstrip antennas," in *IEEE AP-S Symp. Dig.,* Los Angeles, CA, June 1981, pp. 19–22.

Rajan P. Parrikar was born in Goa, India. He received the B.E. degree from the University of Bombay, India, in 1988, the M.S. degree from the University of Mississippi, University, MS, in 1990, and the Ph.D. degree from the University of Colorado at Boulder, in 1993, all in electrical engineering.

He joined the Antenna Engineering Department at Space Systems/Loral, Palo Alto, CA, in 1994, where he has been involved in the design of the phased-array antenna system for the worldwide Globalstar LEO satellite configuration. His research interests are in electromagnetic theory and its application and mathematical methods.

Kuldip C. Gupta (M'62–SM'74–F'88) received the B.E. and M.E. degrees in electrical communication engineering from the Indian Institute of Science, Bangalore, India, in 1961 and 1962, respectively, and the Ph.D. degree from the Birla Institute of Technology and Science, Pilani, India, in 1969.

He has been at the University of Colorado since 1983, initially as a Visiting Professor and later as a Professor. Presently, he is also the Associate Director for the NSF I/UCR Center for Advanced Manufacturing and Packaging of Microwave, Optical, and Digital Electronics (CAMPmode) at the University of Colorado. Earlier, he was at the Indian Institute of Technology, Kanpur (IITK) (1969–1975), where he was a Professor in electrical engineering. On leave from IITK, he was a Visiting Professor at the University of Waterloo, Canada, the Ecole Polytechnique Federale de Lausanne, Switzerland, the Technical University of Denmark (Lyngby), the Eidgenossische Technische Hochschule, Zurich, and the University of Kansas, Lawrence. From 1971 to 1979, he was the Coordinator for the Phased-Array Radar Group of the Advanced Center for Electronics Systems at the Indian Institute of Technology. On sabbatical from the University of Colorado from 1993 to 1994, he was a Visiting Professor at the Indian Institute of Science in Bangalore and a Consultant at the Indian Telephone Industries, Bangalore. He is the author or coauthor of six books: *Microwave Integrated Circuits* (New York: Wiley, 1974); *Microstrip Line and Slotlines* (Norwood, MA: Artech House, 1979); *Microwaves* (New York: Wiley, 1979); *CAD of Microwave Circuits* (Norwood, MA: Artech House, 1981); *Microstrip Antenna Design* (Norwood, MA: Artech House, 1988); and *Analysis and Design of Planar Microwave Components* (New York: IEEE Press, 1994). Also, he has contributed chapters to *Handbook of Microstrip Antennas* (London, U.K.: Peter Peregrinus, 1989); *Handbook of Microwave and Optical Components, Vol. 1* (New York: Wiley, 1989); *Microwave Solid State Circuit Design* (New York: Wiley, 1988); and to *Numerical Techniques for Microwave and Millimeter Wave Passive Structures* (New York: Wiley, 1989). He has published more than 170 research papers and holds three patents in the microwave area. His current research interests are in the area of computer-aided design techniques for microwave and millimeter-wave integrated circuits and integrated antennas.

Dr. Gupta is a Fellow of the Institution of Electronics and Telecommunication Engineers (India), a member of USRI (Commission D, USA), and a member of the Electromagnetics Academy (MIT). He is a member of the ADCOM for the Microwave Theory and Techniques (MTT) Society of IEEE, a co-chair of the IEEE MTT-S Technical Committee on CAD (MTT-1), a member of the IEEE Technical Committee on microwave field theory (MTT-15), and is on the Technical Program Committees for MTT-S International Symposia. He is the Founding Editor of the *International Journal of Microwave and Millimeter-Wave Computer-Aided Engineering* since 1991. He is on the editorial boards of IEEE TRANSACTIONS ON MICROWAVE THEORY OF TECHNIQUES, *Microwave, and Optical Technology Letters*, *International Journal of Numerical Modeling*, and three journals of IETE (India). He is listed in *Who's Who in America*, *Who's Who in the World*, *Who's Who in Engineering*, and *Who's Who in American Education.*